Electronic Supplementary Material (ESI) for Physical Chemistry Chemical Physics.


**Supplementary Figures for:**

# Average orientation of a fluoroaromatic molecule in lipid bilayers from DFT-informed NMR measurements of $^{1}$H-$^{19}$F dipolar couplings

Eleri Hughes, John Griffin, Michael P. Coogan and David A. Middleton

Department of Chemistry, Lancaster University, Lancaster, United Kingdom LA1 4YB

Corresponding author:

David A. Middleton

E-mail: d.middleton@lancaster.ac.uk

Telephone: +44 1524 594328

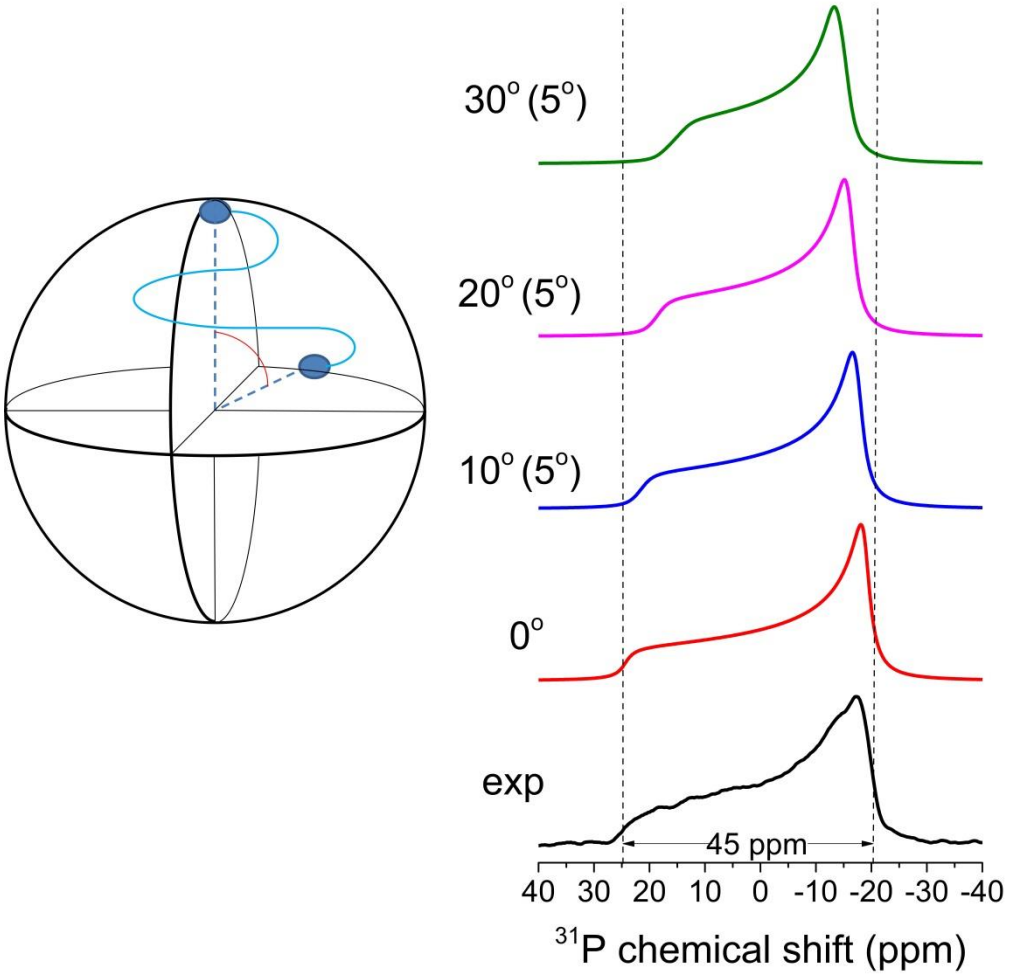


Figure S1. Experimental (black) $^{31}$P powder pattern of DMPC bilayers containing FBTA (20:1 molar ratio of lipid to drug) at 30°C. The full-width anisotropy of 45.2 ppm is typical for rotational averaging of the DMPC $^{31}$P chemical shift tensor within multilamellar vesicles. The coloured spectra are simulations representing different angular excursions of the lipids (mean +/- a standard deviation of 5°) from an initial position as a result of rapid lateral diffusion or vesicle tumbling (left diagram). Even relatively a small angular excursion of 10° gives rise to measureable narrowing of the powder line width, and further displacements also cause a distortion of the powder line shape. Hence lateral diffusion and vesicle tumbling do not influence the $^{31}$P line shape for the mixed DMPC/FBTA system.

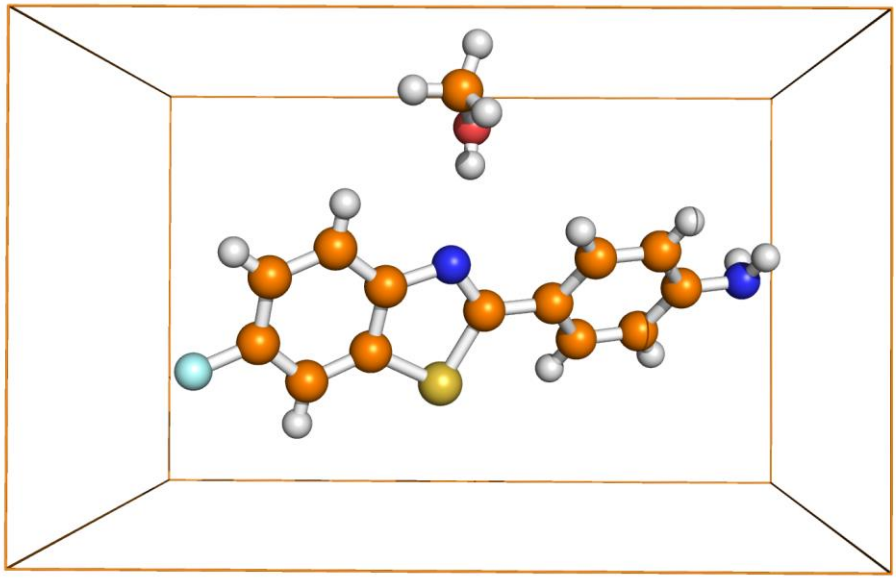

Figure S2. X-ray crystal structure of the methanol solvate of FBTA, $C_{14}H_{13}FN_2OS$ (*M* =276.32 g/mol): orthorhombic, space group Pbca (no. 61), *a* = 9.54533(14) Å, *b* = 14.9685(2) Å, *c* = 17.9615(3) Å, *V* = 2566.33(7) Å$^3$, *Z* = 8, *T* = 100.01(10) K, μ(CuKα) = 2.302 mm$^{-1}$, *Dcalc* = 1.430 g/cm$^3$, 21876 reflections measured (9.848° ≤ 2Θ ≤ 153.51°), 2691 unique ($R_{int}$ = 0.0460, $R_{sigma}$ = 0.0203) which were used in all calculations. The final $R_1$ was 0.0379 (I > 2σ(I)) and $wR_2$ was 0.1089 (all data). The crystal structure is deposited at the Cambridge Crystallographic Data Centre (CCDC 1584785).

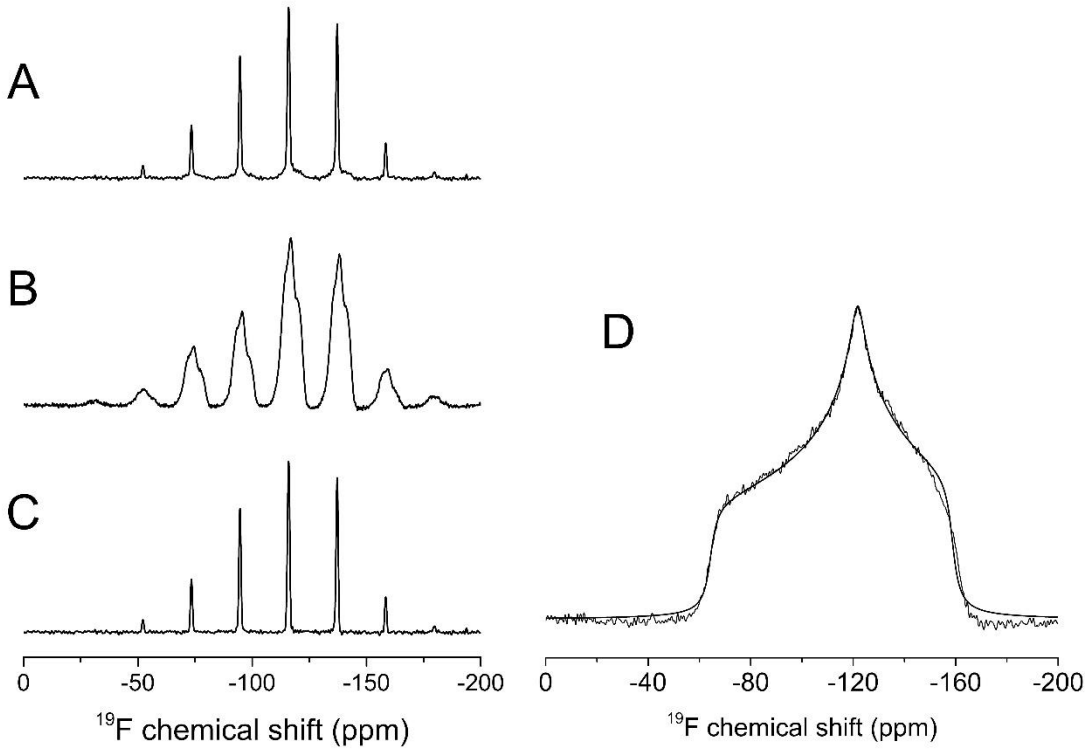


Figure S3. Proton-decoupled $^{19}F$ solid-state NMR spectra of FBTA. Cross-polarisation magic-angle spinning (CP-MAS) spectra (obtained with 8 kHz sample spinning) are shown for (A) the FBTA methanol solvate recrystallised from methanol as for the X-ray analysis, (B) FBTA recrystallised from ethanol:water and (C) the methanol solvate after subtraction of the spectrum of the ethanol:water form (scaled appropriately) to remove the small broad component close to the base line. It is estimated that the broad component represents 5 % of the total FBTA. The spectrum of the ethanol:water form is consistent with $Z' \geq 3$. D: Static, non-spinning spectrum of the FBTA methanol solvate (corrected as described above) overlaid with the calculated best-fitting powder pattern corresponding to the CSA principal values in Table 1 of the main text.

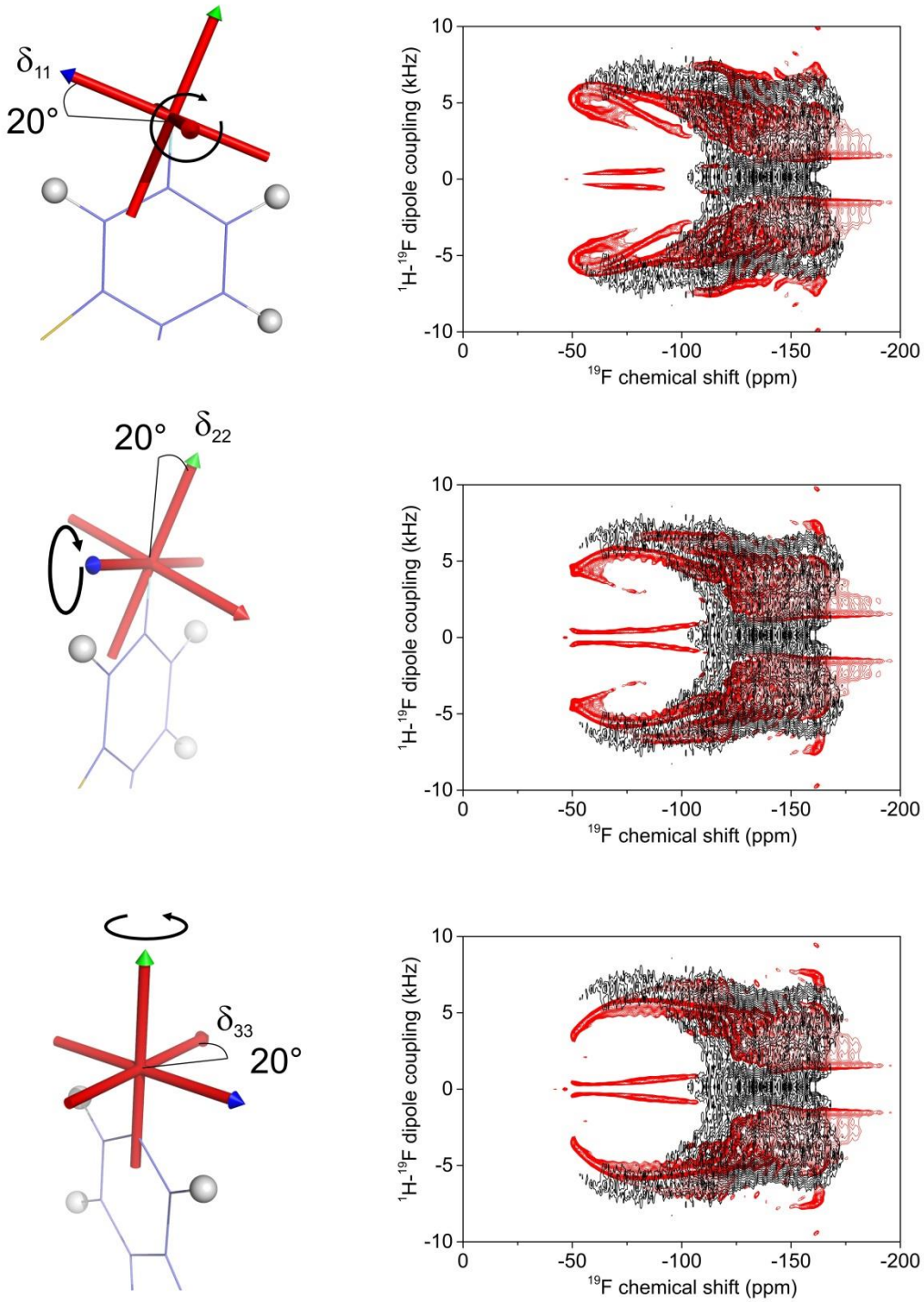


Figure S4. The experimental $^{1}H$-$^{19}F$ PISEMA spectrum (black) of FBTA in DMPC-$d_{54}$ bilayers (reproduced from the main text) overlaid with simulated spectra (red) for 20° excursions of each principal axis of the chemical shielding tensor from the positions calculated by CASTEP and shown in Figure 3 of the main text.

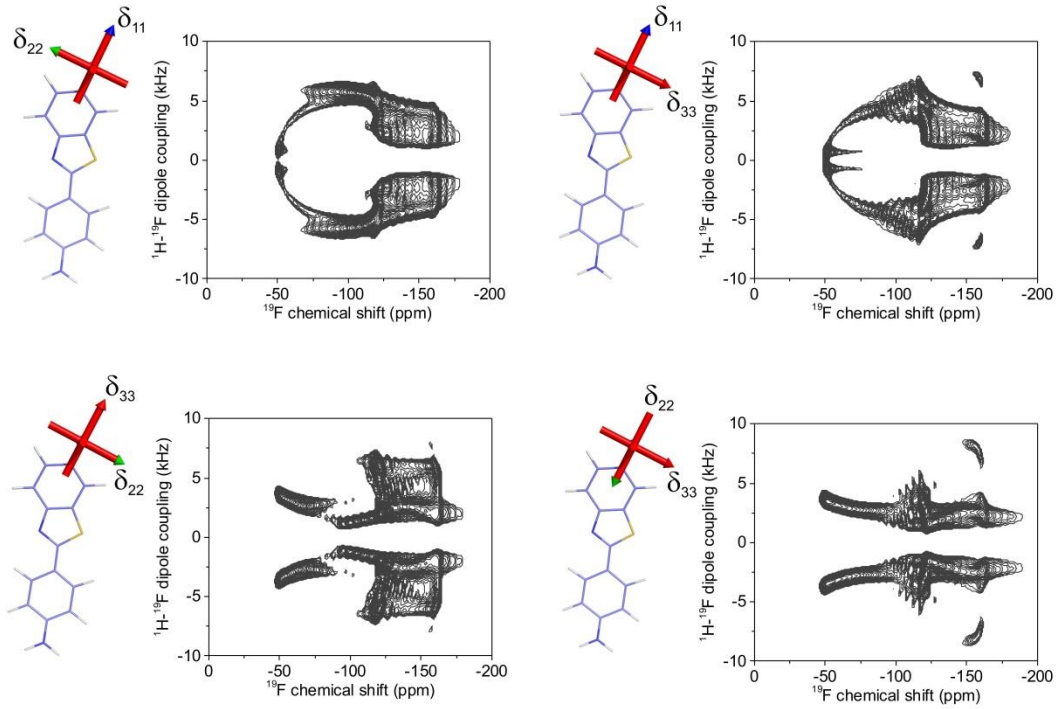


Figure S5. Simulated $^{1}$H-$^{19}$F PISEMA spectra based on the$^{1}$H-$^{19}$F dipole couplings and $^{19}$F CSA of FBTA, with $\delta_{11}$ and $\delta_{22}$ aligned along the C-F bond and with either $\delta_{22}$ or $\delta_{33}$ in the plane of the aromatic ring.

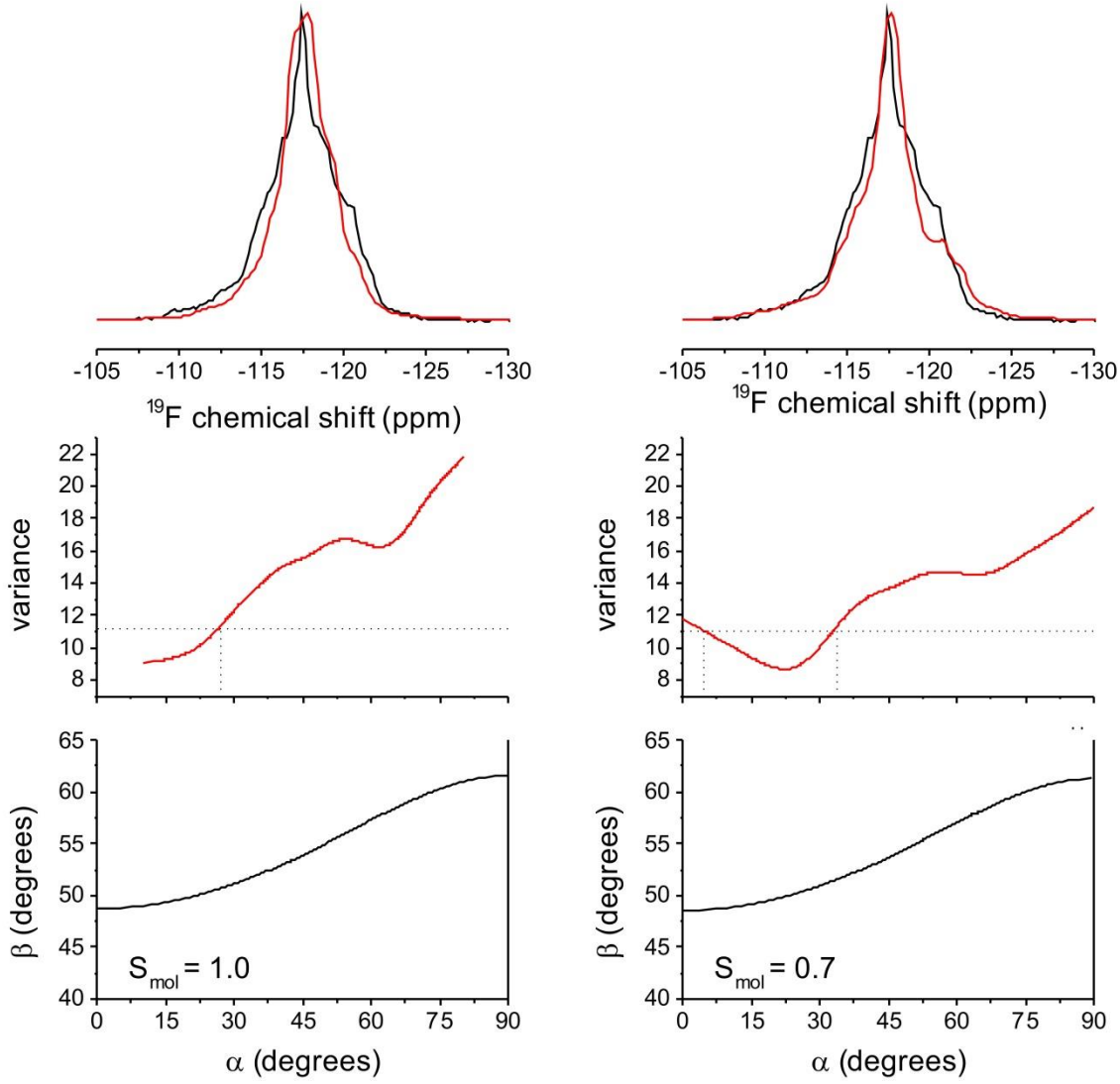


Figure S6. Bottom: a quadrant of the plot in Figure 2E of the main text, showing the combinations of angles $\alpha$ and $\beta$ consistent with the measure range of $\Delta\delta_{av}$ of 1.05 - 1.25 ppm for different values of the order parameter $S_{mol}$. Middle: Plots of the variance (chi-square) of simulated proton-coupled $^{19}F$ NMR spectra from the experimental spectrum for each permitted combination of $\alpha$ and $\beta$. Top: The experimental spectrum (black) overlaid with the simulated spectra in closest agreement (corresponding to the minimum variance) at each value of $S_{mol}$. Chi-square values of less than 11 corresponded to the closest agreement with the data.

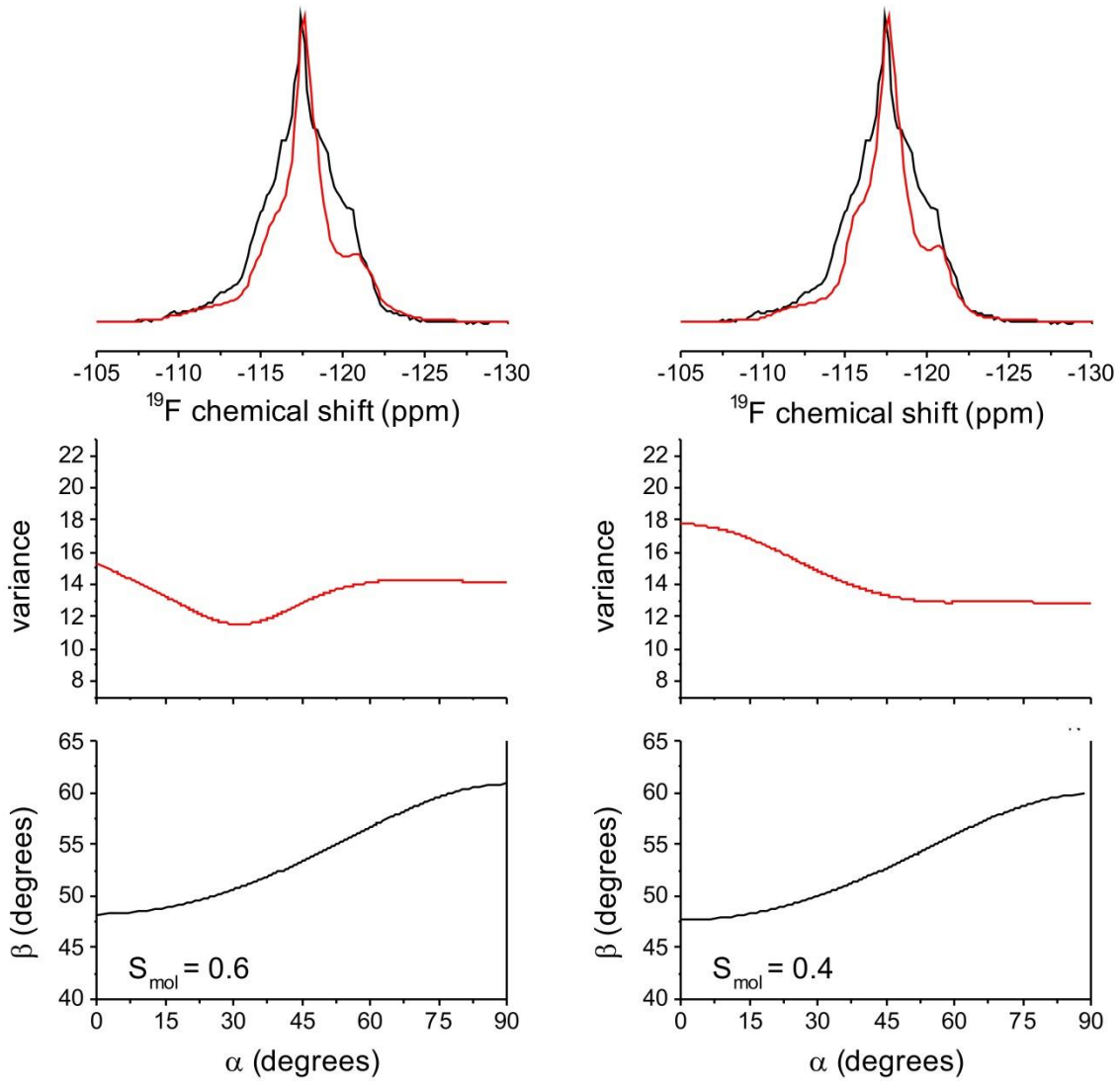


Figure S7. Continuation of Figure S6 for values of $S_{mol}$ of 0.6 and 0.4. At $S_{mol}$ values less than 0.7, the simulated spectra are noticeably narrower than the experimental spectra.

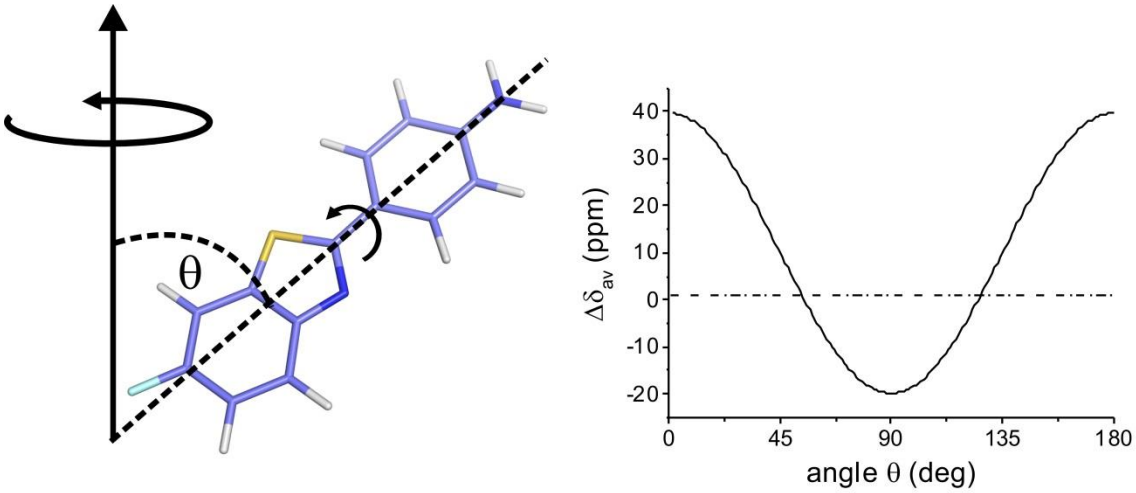


Figure S8. The effect of internal motion on the averaged $^{19}$F CSA, $\Delta\delta_{av}$. Rotation about the bond between the two ring systems was considered simultaneously with whole molecule rotation about an axis collinear with the bilayer normal. Internal rotation results in a scaled, axially symmetric CSA with the principal axis projected along the axis of internal rotation. Molecular rotation further averages the CSA by $(3\cos^2\theta\text{-}1)/2$, where $\theta$ is the tilt angle of the molecule relative to the bilayer normal. Under these conditions (and assuming $S_{mol}$ = 1.0 in the first instance), the closest agreement with the observed $\Delta\delta_{av}$ range of 1.05-1.25 ppm occurs when $\theta$ = 51° or 129°.